Journal of ELECTRONIC MATERIALS, Vol. 37, No. 6, 2008
DOI: 10.1007/s11664-008-0409-4

Some Practical Issues of Curvature and Thermal Stress in Realistic Multilevel Metal Interconnect Structures

T.-S. PARK,[1,4] M. DAO,[1] S. SURESH,[1] A.J. ROSAKIS,[2] D. PANTUSO,[3] and S. SHANKAR[3]

1.—Department of Materials Science and Engineering, Massachusetts Institute of Technology, Cambridge, MA 02139, USA. 2.—Graduate Aeronautical Laboratories, California Institute of Technology, Pasadena, CA 91125, USA. 3.—Technology CAD Group, Intel Corporation, Hillsboro, OR 97124, USA. 4.—e-mail: jypark38@alum.mit.edu

This paper presents the results of a systematic study of curvature and stress evolution during thermal loading in single- and multilevel interconnect line structures which have been deposited on a much thicker substrate. Effects of line aspect ratio, passivation geometry, and metal density within a metalization level on thermal stress evolution in the lines are addressed. The current analytical stress model enables us to predict that interaction between lines on the same level, i.e., in the lateral direction, is so strong that it cannot be neglected. A two-dimensional (2-D) finite element method has been used to verify the accuracy of the current model, while available experimental data have been compared with theory. In order to capture the exact variation of the thermal stresses at different metalization levels, and to investigate the effect of the upper level line arrangements on the stress states at the lower level, a three-dimensional (3-D) finite element analysis was employed. It can be seen that the interaction between levels in the vertical direction is quite weak when the thickness of the interlevel dielectric (ILD) layer becomes comparable to that of the metal layer.

Key words: Copper, curvature, multilevel metalization, thermal stress, thin-film structure

INTRODUCTION

It is desirable to evaluate stresses in interconnect lines formed on a Si substrate to improve the design of the device structure, selection of materials, fabrication processes, and other aspects of the device to enhance its manufacturability and reliability. Stress measurements can be used to facilitate quality control during various fabrication steps including film deposition, patterning, polishing, and thermal cycling due to repeated annealing and curing steps. Determining stress values in the lines also enables us to assess the reliability of the interconnect materials against failure from such phenomena as electromigration,[1–3] stress-induced voiding,[4,5] and hillock formation.[6] As new, low-modulus, high-porosity insulating materials are introduced because of their low dielectric constants, additional failure mechanisms, such as yielding and cracking in the dielectric layer embedding the metal lines and in the interface between the two, are also observed.[7]

The stresses in the interconnect structure may result from various sources. One of the major factors affecting reliability stems from stresses produced by thermal mismatch between metal lines and surrounding materials. Various experiments based on X-rays[8] and substrate curvature measurements[9–11] have been performed for the case of film structures containing metal lines embedded within dielectric materials. In parallel, finite element analysis (FEA) has been employed to estimate volume-averaged stresses in metal lines.[12–14] Although FEA can incorporate detailed information of the metal lines, including inelastic material properties and/or geometry of barrier layers,[14] it usually requires lengthy computations, which must generally be

(Received August 27, 2007; accepted February 12, 2008; published online March 18, 2008)

repeated each time the line geometry is changed. In contrast, analytical predictions provide very good insight into the parameter controlling the deformation process, and also provide reasonably accurate results in a time-efficient manner.[15–17] Using Eshelby's inclusion theory, Niwa et al.[15] modeled the line as a cylinder of elliptical cross-section embedded in an infinite isotropic matrix having the same elastic properties as the line. This model was generalized by Korhonen et al.[16] by using different elastic properties between the line and the matrix while still neglecting the substrate. These early analyses, based on Eshelby's theory, can incorporate aspect ratios of the lines, but fail to capture the effects of the substrate and of the neighboring lines, while completely neglecting sharp edges/corners of the lines. Wikström et al.[17] were the first to propose a fully fledged thermoelastic analysis of periodic, alternating, metal/dielectric lines on a substrate. This model considered the two limiting cases, low and high line aspect ratios, which is similar to the analysis employed in the present work. Wikström's model, however, did not account for substrate deformation, and as a result, was unable to provide wafer curvature information, which is directly related to the volume-averaged stresses in both the metal and the dielectric lines on the substrate. This model was also strictly developed for a single-level structure deposited on a much thicker substrate.

As the industry is pushing for ever-increasing levels of metalization (a great need for more integrated semiconductor chips), the need for multilevel stress analysis tools is also becoming imminent. Nevertheless, very little work has been done, on both analytical and numerical modeling, of multilevel thin-film/substrate systems. In perhaps the first of these studies, Shen[18] presented numerical results on the evolution of thermal stresses in very simple multilevel structures. Two levels of metal lines, aligned vertically or arranged in a staggered manner, were modeled using two-dimensional (2-D) FEA. This analysis quantitatively estimated interactions between upper and lower metalization levels. Due to limitation of a 2-D analysis, it could not properly take into account a truly three-dimensional (3-D), realistic, multilevel line geometry having different line directions at each level. Furthermore, there was no attempt to relate wafer curvature to feature stress. Such a relation is very important for process control in all stages of metalization (e.g., chemical-mechanical polishing (CMP) following each metalization step).[19]

In the present work, wafer curvatures as well as volume-averaged stresses in lines are calculated for alternating metal/dielectric lines on a substrate during temperature changes. This incorporates the stress-curvature relation and additional conditions relevant to limiting line geometry. Two limiting cases are considered. The first is relevant when line aspect ratios are very low. In this case, each line can be considered an individual film. In contrast, when the aspect ratios are sufficiently high, the metal and dielectric lines can be modeled as a homogeneous but anisotropic composite layer with different effective thermoelastic properties along and across the lines. Numerical analysis using 2-D FEA has been employed to evaluate the validity of the theoretical predictions for these two limiting cases. Furthermore, 3-D FEA was carried out for the purpose of capturing the realistic, three-dimensional nature of multilevel structures and of exploring the possibility of extending the analysis to more complicated line geometries. Finally, available experimental results have been compared with both analytical and numerical predictions.

The ultimate purpose of this paper is a practical one. Its goal is to demonstrate that analysis of the type described in the above can indeed be appropriately generalized to cover realistic multilevel film structures of practical interest in integrated circuit (IC) manufacturing. The detailed comparisons of analytically computed stresses to the 2-D and the 3-D numerical simulations establish the limitations of the purely closed-form, but approximate, analytical approach. They also establish the range of its applicability to practical stress problems in more realistic structures.

ANALYTICAL MODEL

Single-Level Structure

Low Line Aspect Ratio

When metal and dielectric lines are very short and wide (Fig. 1a) each line can be treated as an individual thin layer (Fig. 1b).[17] Since the lines are very wide across the line direction, and the line height is very small compared to both its length and width, the stress state in the lines is basically that of equibiaxial plane stress. Therefore, the volume-averaged stress values along the line (x-direction), and across the line (y-direction) are the same, as are the curvatures in the x- and y-directions, for this limiting line geometry. From force and moment balance equations of the metal thin-layer structure,[20,21] the volume-averaged stresses from thermal mismatch in the metal line, $\langle\sigma^{\mathrm{l}}\rangle$, and the curvature changes of the metal/substrate structure, $\Delta\kappa^{\mathrm{l}}$, during a temperature change, ΔT, can be expressed as,

$$\langle\sigma^{\mathrm{l}}_{xx}\rangle = \langle\sigma^{\mathrm{l}}_{yy}\rangle = -\overline{E_{\mathrm{l}}}(\alpha_{\mathrm{l}} - \alpha_{\mathrm{s}})\Delta T, \quad \langle\sigma^{\mathrm{l}}_{zz}\rangle = 0, \tag{1}$$

$$\Delta\kappa^{\mathrm{l}}_{x} = \Delta\kappa^{\mathrm{l}}_{y} = \frac{6}{\overline{E_{\mathrm{s}}}}\frac{h}{h_{\mathrm{s}}^2}\overline{E_{\mathrm{l}}}(\alpha_{\mathrm{s}} - \alpha_{\mathrm{l}})\Delta T, \tag{2}$$

where $\overline{E_{\mathrm{l}}}$ and α_{l} are the biaxial modulus ($E_{\mathrm{l}}/[1 - \nu_{\mathrm{l}}]$) and thermal expansion coefficient of the thin metal layer, respectively, $\overline{E_{\mathrm{s}}}$ and α_{s} are the corresponding properties of the substrate, and h and h_{s} are the thickness of the layer and the substrate, respectively. Similar expressions can be obtained for the

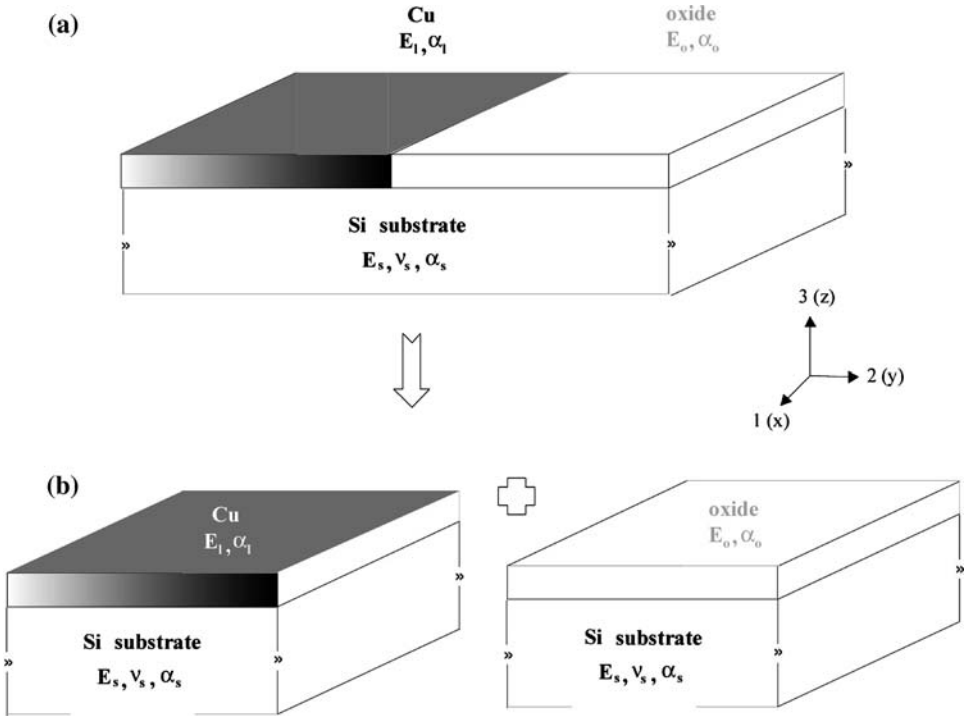

Fig. 1. Schematic of Cu interconnect lines without a passivation layer on a Si substrate following the Damascene process at low line aspect ratio.

volume-averaged stresses in the dielectric line, $\langle \sigma^o \rangle$, and the curvature changes of the dielectric/substrate structure, $\Delta\kappa^o$, with corresponding thermoelastic properties of the dielectric lines. The overall curvature changes of both the metal and dielectric layers on the substrate (Fig. 1a) are simply the sum of contributions from each layer (Fig. 1b).

High Line Aspect Ratio

Figure 2a is a schematic of metal interconnect lines (e.g., copper) with dielectric lines (e.g., oxide) on a Si substrate following the Damascene process. Assuming that the aspect ratio (h/w) of the metal and dielectric lines is sufficiently high, the structure can be homogenized into a composite layer as shown in Fig. 2b.[17,22] Due to the anisotropic line geometry, this composite layer has different values of effective elastic modulus and thermal expansion coefficient along the lines, E_x and α_x, respectively, from those across the lines, E_y and α_y, respectively, even if the material itself is modeled as elastically and thermally isotropic. Using composite theory, these effective properties can be calculated in terms of the volume fraction, elastic modulus, and thermal expansion coefficient of the metal lines, f_l (= w/p), E_l and α_l, and those of dielectric lines, f_o (= $1 - w/p$), E_o, and α_o.[22]

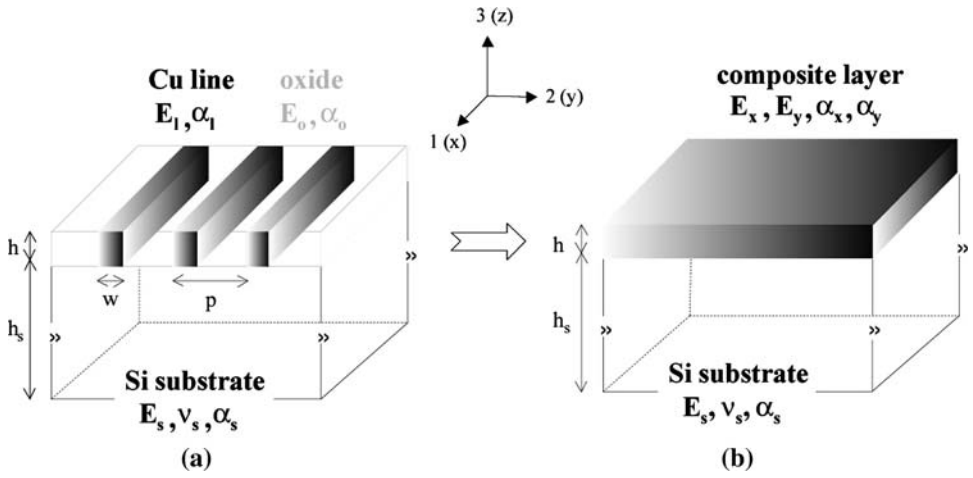

Fig. 2. Schematic of Cu interconnect lines without a passivation layer on a Si substrate following the Damascene process at high line aspect ratio.

Park and Suresh[22] proposed a simple uniaxial, anisotropic composite model for patterned elastic lines to predict curvature evolution in response to changes in internal stresses arising from thermal cycling. Their model provides reasonably accurate values compared to detailed finite element analysis. The curvature changes of the wafer along and across the lines, $\Delta\kappa_x$ and $\Delta\kappa_y$, respectively, during a temperature change, ΔT, are expressed as,

$$\Delta\kappa_x = \frac{6}{E_s}\frac{h}{h_s^2}E_x(\alpha_s - \alpha_x)\Delta T, \tag{3}$$

$$\Delta\kappa_y = \frac{6}{E_s}\frac{h}{h_s^2}E_y(\alpha_s - \alpha_y)\Delta T. \tag{4}$$

By convention, a positive curvature change results in a concave shape of the line structure (composite layer) side of the substrate. When the layer is much thinner than the substrate, the volume-averaged normal stresses in the entire layer along and across the lines, $\langle\sigma_{xx}\rangle$ and $\langle\sigma_{yy}\rangle$, respectively, can be obtained from curvature changes during a thermal excursion using an anisotropic form of the well-known Stoney formula.[23,24] Since the thickness of the layer is much less than that of the substrate, the net out-of-plane average stress, $\langle\sigma_{zz}\rangle$, in the layer vanishes. In the limit of high aspect ratio, the average normal strains on the x–z plane for both metal and dielectric lines should be the same (isostrain condition; $\langle\epsilon_{xx}^{l}\rangle = \langle\epsilon_{xx}^{o}\rangle$ and $\langle\epsilon_{zz}^{l}\rangle = \langle\epsilon_{zz}^{o}\rangle$).[17,25] In addition, equilibrium consideration shows that the averaged stresses in the y-direction for both lines must be equal (isostress condition; $\langle\sigma_{yy}^{l}\rangle = \langle\sigma_{yy}^{o}\rangle$).[17,25]

By employing the above conditions, the volume-averaged stresses in the metal and dielectric lines can be computed from the following matrix equation:

$$\begin{bmatrix} f_l & 0 & 0 & f_o & 0 & 0 \\ 0 & f_l & 0 & 0 & f_o & 0 \\ 0 & 0 & f_l & 0 & 0 & f_o \\ \frac{1}{E_l} & -\frac{\nu_l}{E_l} & -\frac{\nu_l}{E_l} & -\frac{1}{E_o} & \frac{\nu_o}{E_o} & \frac{\nu_o}{E_o} \\ -\frac{\nu_l}{E_l} & -\frac{\nu_l}{E_l} & \frac{1}{E_l} & \frac{\nu_o}{E_o} & \frac{\nu_o}{E_o} & -\frac{1}{E_o} \\ 0 & 1 & 0 & 0 & -1 & 0 \end{bmatrix} \begin{bmatrix} \langle\sigma_{xx}^{l}\rangle \\ \langle\sigma_{yy}^{l}\rangle \\ \langle\sigma_{zz}^{l}\rangle \\ \langle\sigma_{xx}^{o}\rangle \\ \langle\sigma_{yy}^{o}\rangle \\ \langle\sigma_{zz}^{o}\rangle \end{bmatrix} = \begin{bmatrix} \Gamma(\Delta\kappa_x + \nu_s\Delta\kappa_y) \\ \Gamma(\nu_s\Delta\kappa_x + \Delta\kappa_y) \\ 0 \\ (\alpha_o - \alpha_l)\Delta T \\ (\alpha_o - \alpha_l)\Delta T \\ 0 \end{bmatrix}, \tag{5}$$

where $\Gamma = \frac{1}{6}\frac{h_s^2}{h}\frac{E_s}{1-\nu_s^2}$ and $\Delta\kappa_x$, $\Delta\kappa_y$ are the net substrate curvature changes in the two orthogonal directions, parallel and perpendicular to the lines that are associated with a change of temperature ΔT. In this formula h is the height of the lines within the periodic structure (without a capping layer).

Since this is for the limiting conditions of a very high aspect ratio, this model does not account for the effect of line aspect ratio. In addition, at high aspect ratio, each line is contacted on its top in a very limited region with a passivation layer which is deposited during postprocessing. As a result, the present model, which does not take into account a capping layer, is still expected to yield accurate stress predictions irrespective of postprocessing. Indeed, as integration of semiconductor devices increases, and the line aspect ratio becomes higher, this theory becomes progressively more practical for calculation of volume-averaged stresses in interconnect lines.

Multilevel Structure

The evolution of curvatures of a multilevel structure can also be assessed using the above model by invoking the concept of superposition. Figure 3 shows a schematic of two trilayer structures with different metal line arrangements on the upper level. One is an aligned structure with lines on the upper level running in the same direction as those on the lower level (Fig. 3a). The other is a perpendicular structure with lines on the upper level running in a perpendicular direction to the lower-level lines (Fig. 3b), which is a more realistic line arrangement in the semiconductor interconnect design. In the high-aspect-ratio limit, each structure can be regarded as the superposition of two composite layers, with an interlevel dielectric layer (ILD) between them. For a given ILD material, the curvature change resulting from the ILD layer, $\Delta\kappa_p$, is obtained in terms of the biaxial modulus of the ILD layer, $\overline{E_p}(= E_p/[1-\nu_p])$, its thermal expansion coefficient, α_p, and its thickness, h_p, as,

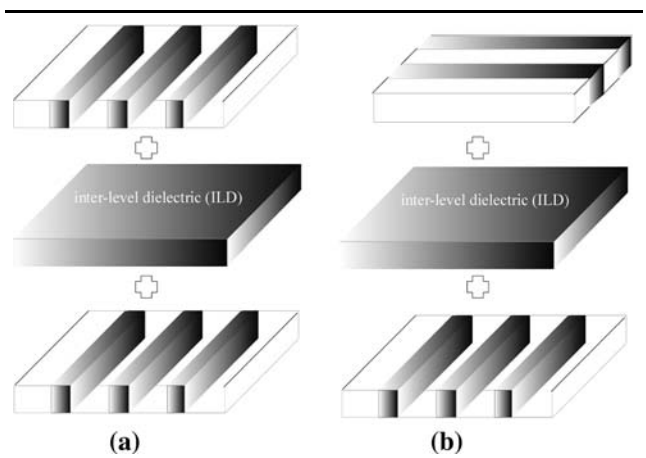

Fig. 3. Superimposition of individual metal and ILD layers resulting in a trilayer structure after the dual Damascene process: (a) aligned structure and (b) perpendicular structure.

$$\Delta\kappa_p = \frac{6}{\overline{E_s}}\frac{h_p}{h_s^2}\overline{E_p}(\alpha_s - \alpha_p)\Delta T. \quad (6)$$

By adding $\Delta\kappa_p$ from the ILD layer (Eq. 6) to the values of $\Delta\kappa_x$ and $\Delta\kappa_y$ from the two composite layers (Eqs. 3 and 4), respectively, the curvature changes of this trilayer structure, $\Delta\kappa'_x$ and $\Delta\kappa'_y$, are obtained:

$$\Delta\kappa'_x = \Delta\kappa_x(\text{lower layer}) + \Delta\kappa_p(\text{ILD layer}) + \Delta\kappa_x(\text{upper layer}). \quad (7)$$

$$\Delta\kappa'_y = \Delta\kappa_y(\text{lower layer}) + \Delta\kappa_p(\text{ILD layer}) + \Delta\kappa_y(\text{upper layer}). \quad (8)$$

The structure shown in Fig. 3 can be obtained by the dual Damascene process.[19] It may be followed by additional processes such as another passivation layer deposition and further metalization. The concept of superposition can be applied to structures with more than three layers provided that linear elastic conditions are maintained.

FINITE ELEMENT METHOD

The finite element method (FEM) was used to verify the present analytical model. For this purpose, the finite element program ABAQUS[26] was employed. Table I shows the material properties used in the simulations.[13,23] In this work Cu and SiO_2 were chosen as the model metal and dielectric materials, respectively, in light of the shift from conventional Al-based interconnects to new Cu Damascene structures in the semiconductor industry. Isotropic material properties were used and residual stresses, which may result from Cu deposition and/or polishing, were not taken into account. This analysis deals only with elasticity, which is expected to be valid over a wide range of practical interest since the material surrounding the Cu lines, especially in the case of passivated lines, leads to elevated levels of hydrostatic stress in the lines, thereby inducing constrained deformation.[9]

2-D Generalized Plane-Strain Model

A unit cell illustrating the mesh used in the 2-D numerical simulation is shown in Fig. 4. Due to the periodicity and symmetry of the arrangement, only a unit segment ranging from a symmetry axis and the neighboring periodic boundary is needed. Here h, w, and p represent the height, width, and pitch of the Cu lines, respectively. At the reference point 0 ($y = 0$, $z = 0$) in Fig. 4, the displacements along the y- and z-directions are taken to be zero. Along the symmetry axis ($y = 0$), the displacement in the y-direction vanishes. This means

$$u_y = 0 \quad \text{at} \quad y = 0. \quad (9)$$

The outer boundary of the unit cell ($y = p/2$) is free to move, but it is forced to remain on a straight line following the assumptions of classical bending theory. This gives

$$y = C_1 z + C_2 \quad \text{at} \quad y = \frac{p}{2}, \quad (10)$$

where C_1 and C_2 are constants to be determined with further analysis. No other boundaries are constrained during the thermally induced deformation. The wafer curvature change across the lines (in the y-direction) can then be directly calculated from the relative positions of the representative points on the boundary, $y = p/2$;

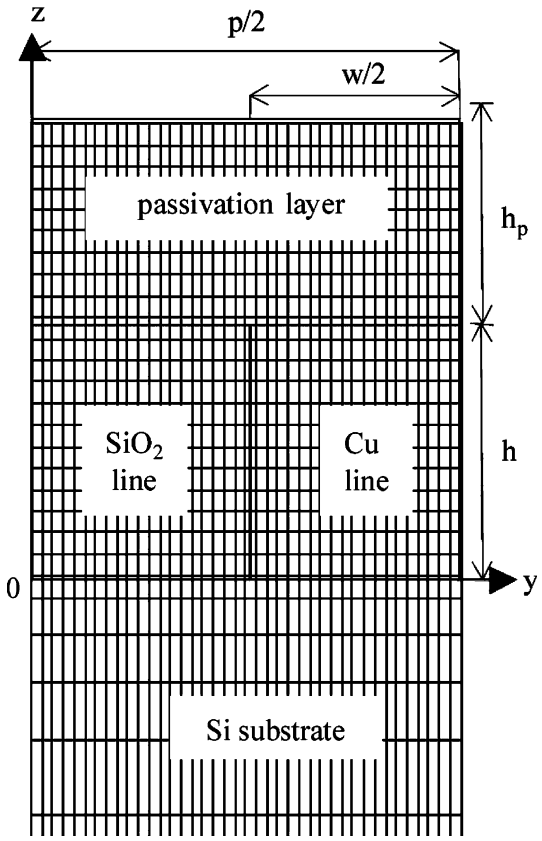

Fig. 4. A representative unit cell (top portion) and finite element discretization for Cu lines with SiO_2 on the single layer for the 2-D generalized plane-strain model.

Table I. Material Properties Used in the Simulations

	E (GPa)	υ	α [10^{-6}/°C]
Si	130	0.28	2.60
Cu	110	0.30	17.0
SiO_2	71.4	0.16	0.524
Si_3N_4	380	0.20	2.25

$$\Delta\kappa_y = \frac{2}{h_s p}\{[u_y]_{y=\frac{p}{2},\, z=-h_s} - [u_y]_{y=\frac{p}{2},\, z=0}\}, \tag{11}$$

where h_s is the thickness of the substrate.

A generalized plane-strain formulation, which is an extension of the plane-strain framework (with the y–z plane being the plane of deformation), is used in the calculations.[12,13] This is done by superimposing a longitudinal strain, ε_{xx}, on the plane-strain state. To properly simulate the actual response of the patterned parallel lines on the substrate, the strain field ε_{xx} is constrained to induce a constant rotation about the y-axis,

$$\frac{\partial^2 u_z}{\partial x^2} = C_3, \tag{12}$$

where C_3 is a constant directly determined by the analysis. The three-dimensional effect can thus be adequately described by the present model. It gives the wafer curvature change in the x-direction:

$$\Delta\kappa_x = \frac{\partial^2 u_z}{\partial x^2}. \tag{13}$$

The generalized plane-strain model is thus capable of yielding more realistic field quantities in both phases than the strict plane-strain formulation.

3-D Model

Representative unit cells with different line arrangements on upper levels used in the 3-D numerical simulation are shown in Fig. 5. As in the 2-D simulation, the periodicity and symmetry facilitate use of only a unit segment ranging from symmetry planes to the neighboring periodic boundaries for calculation. At the reference point 0 ($x = y = z = 0$), the displacements in all the directions are assigned to be zero. On one symmetry plane ($x = 0$), the displacement in the x-direction vanishes. On the other symmetry plane ($y = 0$), all the nodes are fixed in the y-direction.

The outer boundaries of the unit cells ($x = l$ and $y = p/2$) are free to move, but they are forced to remain as flat planes. This can be obtained by contacting the outer surfaces with frictionless, rigid, and flat planes in the model. The curvature change in the x-direction can then be calculated from the

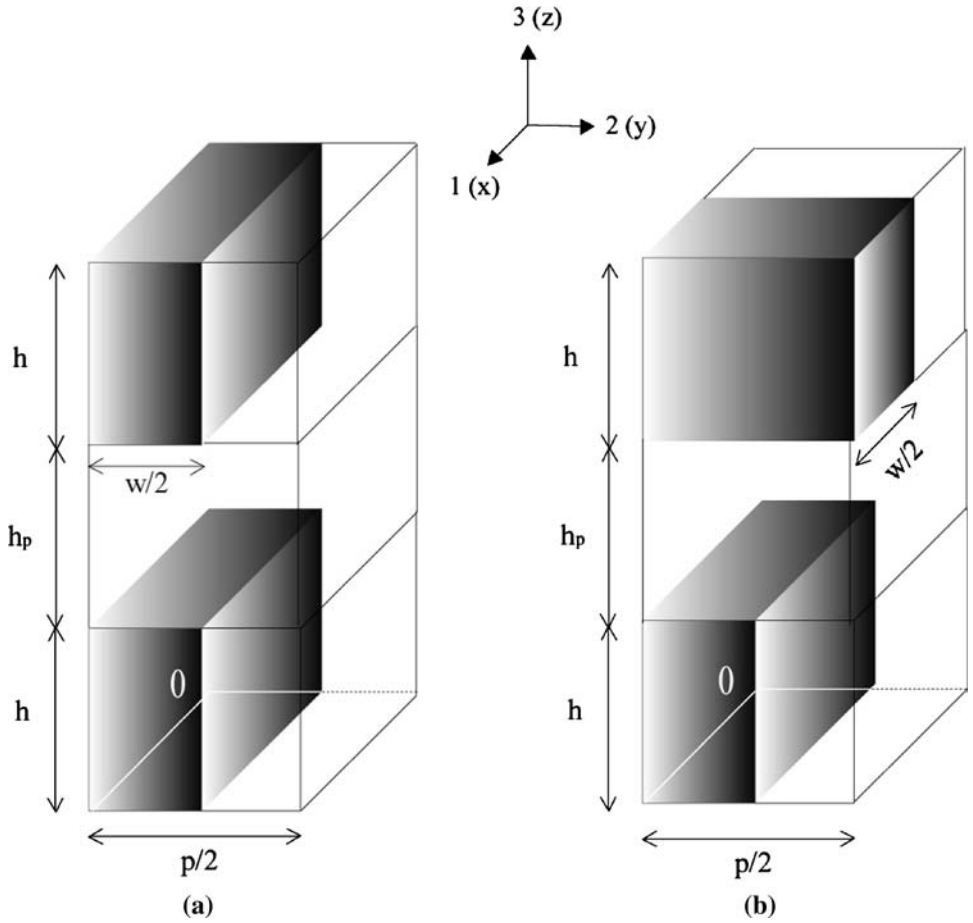

Fig. 5. Representative unit cells (top portion) for Cu lines with SiO_2 on the two level structure after the dual Damascene process for the 3-D finite element model: (a) aligned structure and (b) perpendicular structure.

relative positions of the representative points on the boundary, $x = l$;

$$\Delta\kappa_x = \frac{1}{h_s l}\{[u_x]_{x=l,\, y=\frac{p}{4},\, z=-h_s} - [u_x]_{x=l,\, y=\frac{p}{4},\, z=0}\}. \quad (14)$$

Similarly, the curvature change in the y-direction is obtained from the relative positions of the representative points on the other boundary, $y = p/2$;

$$\Delta\kappa_y = \frac{2}{h_s p}\{[u_y]_{x=\frac{l}{2},\, y=\frac{p}{2},\, z=-h_s} - [u_y]_{x=\frac{l}{2},\, y=\frac{p}{2},\, z=0}\}. \quad (15)$$

In order to confirm the validity of the 3-D FEM, the results from passivated lines on the single-level structure were compared to those from the 2-D generalized plane-strain model. The values for the stress distribution, as well as volume-averaged stresses and wafer curvature changes, were the same in both cases. It was thus established that it is indeed possible to use 3-D FEM for multilevel structure as an extension of 2-D FEM for single-level structure.

RESULTS AND DISCUSSION

Single-Level Structure

Here the current analytical model for stress components on features and overall substrate curvature changes is compared with finite element analysis using a 2-D generalized plane-strain model in various line geometries of varying line aspect ratio (h/w), passivation ratio (h_p/h), and different capping materials. This parametric study is done to investigate the range of validity and of accuracy of our simple analytical model and to identify possible reasons for discrepancies between the theoretical and the numerical predictions. The effect of metal density ($f_l = w/p$) is discussed in the following section. A comparison with available experimental data is also presented.

Curvature Evolution as a Function of Line Aspect Ratios

Figure 6 shows the ratios of the thermal curvature coefficients ($\beta = \Delta\kappa/\Delta T$) between along and across lines, as a function of aspect ratio, at a fixed pitch ratio ($p/w = 2$). In the low-aspect-ratio limit, the lines behave like individual Cu and oxide thin films. The curvature changes in the x- and y-directions are therefore identical. In the high-aspect-ratio limit, it can be seen that the lines collectively constitute a single composite layer with different effective thermoelastic properties, which results in anisotropic curvature values. FEM results are in good agreement with theoretical values at the high aspect ratio limit even down to $h/w = 1$, then approach the other theoretical limit as the aspect ratio becomes lower. Although it is difficult to compare the current analysis to absolute experimental curvature values directly due to the lack of exact thermoelastic property data for Cu and oxide lines in real specimens, comparison of the ratios of curvature changes between along and across the line directions would be useful. Curvature measurements of Damascene Cu lines on a Si substrate with different aspect ratios were previously reported.[11] These values are reasonably matched with the current analytical and numerical results, within experimental scatter, as shown in Fig. 6.

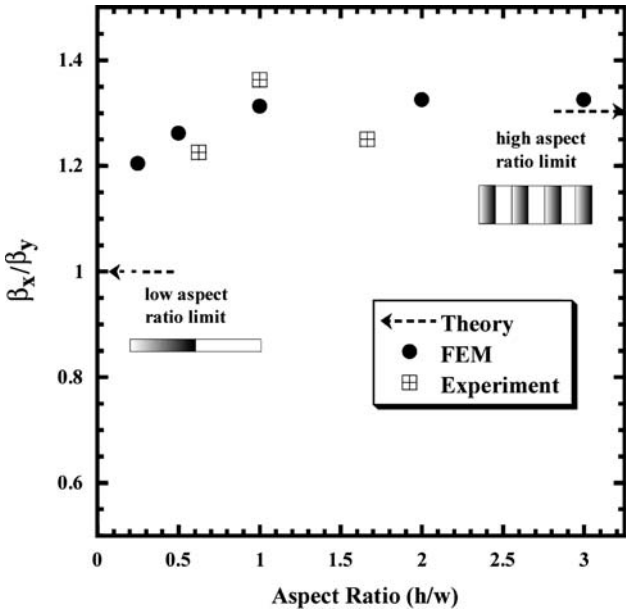

Fig. 6. Ratios of thermal curvature coefficients between along (x) and across (y) line directions of single-level structure without passivation ($w/p = f_l = 0.5$, $h = 1$ μm and $h_s = 525$ μm) as a function of aspect ratio (h/w); low-aspect-ratio limit from Eq. 2 and high-aspect-ratio limit from Eqs. 3 and 4.

Effect of Line and Passivation Geometry on Stress Evolution

Figure 7 illustrates the normal stress components during cooling from 200°C to room temperature (20°C) in Cu lines without passivation (capping) layer as a function of aspect ratio (h/w), at a fixed Cu density ($f_l = 0.5$). In the low-aspect-ratio limit, the Cu lines are so wide that they can be treated as thin, continuous Cu films. Therefore, an equibiaxial plane-stress condition prevails, as shown from Eq. 1. FEM results deviate from the values expected from theory for the intermediate aspect ratios. However, as the aspect ratio increases, these results do approach the theoretical predictions, based on Eq. 5. This is due to the assumption of the current theory that at the high-aspect-ratio limit individual Cu and SiO_2 lines are sufficiently tall so that the additional conditions, i.e., isostrain conditions on the x–z plane and isostress condition in the y-direction, can be used to calculate thermal stresses in each line. From Fig. 7 the theoretical values at the high-aspect-ratio limit underestimate $\langle\sigma^l_{yy}\rangle$,

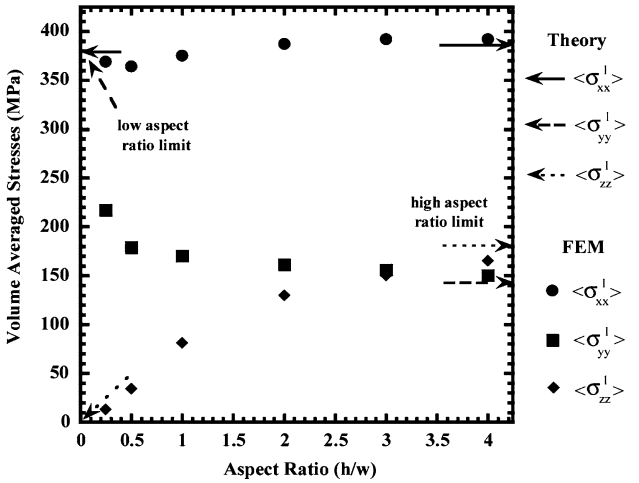

Fig. 7. Volume-averaged stresses in Cu lines on single-level structures without passivation ($w/p = f_l = 0.5$, $h = 1$ μm and $h_s = 525$ μm) as a function of aspect ratio (h/w) during cooling from 200°C to room temperature; low-aspect-ratio limit from Eq. 1 and high-aspect-ratio limit from Eq. 5.

and overestimate $\langle\sigma^l_{zz}\rangle$ compared to FEM results at intermediate line aspect ratios. $\langle\sigma^l_{xx}\rangle$ is well matched over a wide range of aspect ratios. The reason for these discrepancies between theory and FEM will be discussed later, along with the effects of a top passivation, or capping layer.

The variations of normal stress components are shown in Fig. 8 as a function of the thickness of the SiO_2 passivation layer. The $\langle\sigma^l_{xx}\rangle$ values are not heavily influenced by top passivation and correlate quite well with the theory, as shown in Fig. 8a. Values of $\langle\sigma^l_{yy}\rangle$, however, increase with passivation, which leads to a more pronounced deviation in intermediate aspect ratios from the theoretical predictions at the high-aspect-ratio limit (Fig. 8b). Values of $\langle\sigma^l_{zz}\rangle$ also increase when passivated, resulting in better agreement in intermediate aspect ratios with theoretical predictions in the high-aspect-ratio limit, Fig. 8c. For both $\langle\sigma^l_{yy}\rangle$ and $\langle\sigma^l_{zz}\rangle$, there is little difference when the thickness of the passivation layer increases by a factor of 5.

Figure 9 shows contours of σ_{yy} in a Cu line and an oxide trench at various aspect ratios and fixed metal density ($f_l = 0.5$) when passivated with a SiO_2 layer ($h_p/h = 1$). At $h/w = 1$, the Cu line generally shows higher stresses than the oxide trench. When lines are taller ($h/w = 2$), the isostress condition across lines seems valid in the middle of lines and the FEM values in this region are quite well matched with the theoretical prediction from Eq. 5. Near interfaces between underlying/overlying (passivation) layers, however, deviation resulting from thermal mismatch appears. Since SiO_2 is chosen for the overlying layer in this case, localized stresses in the Cu line near an interface between the overlying layer are higher than stress values in the middle of the line. In addition, high localized stress near an interface between the underlying Si substrate are

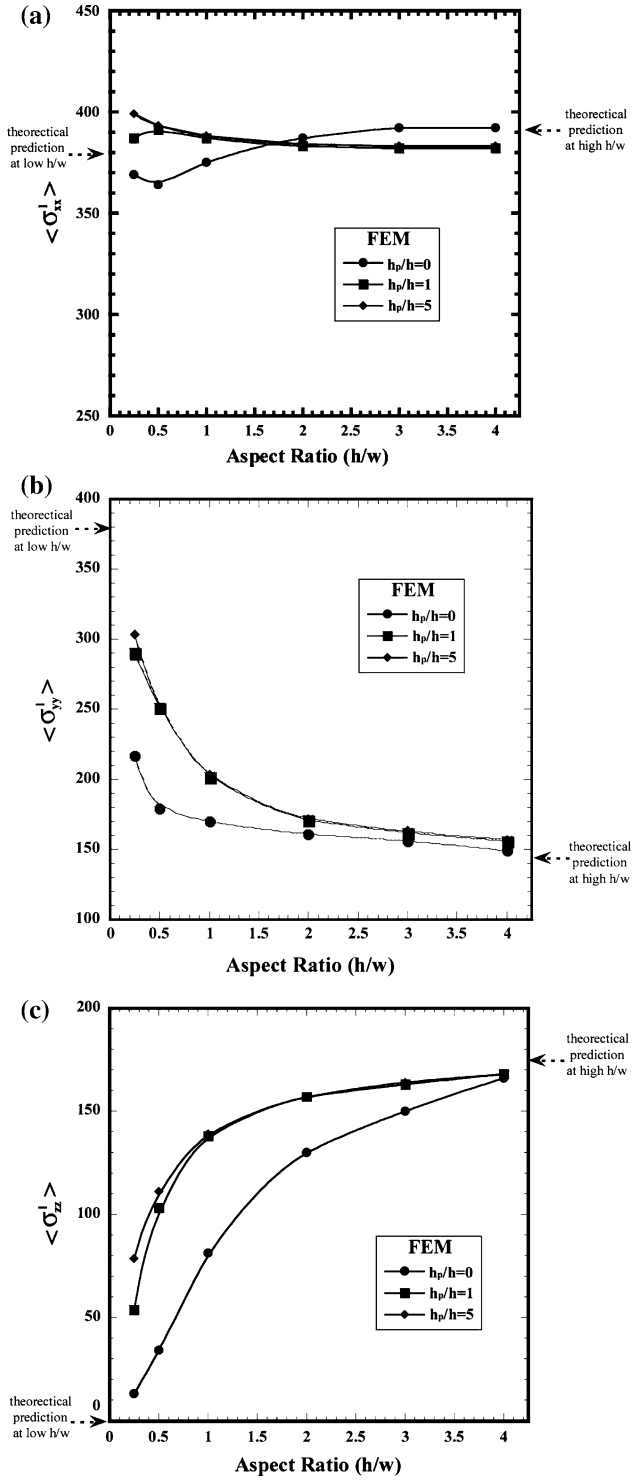

Fig. 8. Volume-averaged stresses in Cu lines on single-level structures with various passivation thicknesses ($w/p = f_l = 0.5$, $h = 1$ μm and $h_s = 525$ μm) as a function of aspect ratio (h/w) during cooling from 200°C to room temperature: (a) $\langle\sigma^l_{xx},\rangle$ (b) $\langle\sigma^l_{yy}\rangle$, (c) $\langle\sigma^l_{zz}\rangle$; low-aspect-ratio limit from Eq. 1 and high-aspect-ratio limit from Eq. 5.

found resulting from large thermal mismatch between the Cu line and the Si substrate. This is why the volume-averaged stresses of Cu lines in the y-direction, $\langle\sigma^l_{yy}\rangle$, exhibit higher values than the

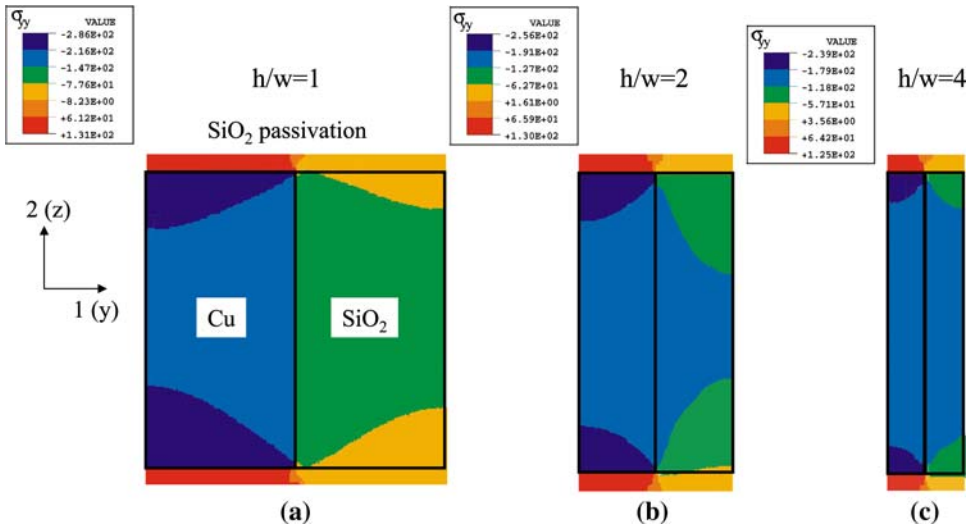

Fig. 9. 2-D FEM contours of stress across lines, σ_{yy}, on single-level structures with SiO_2 passivation layers ($w/p = f_l = 0.5$, $h = 1$ μm, $h_p = 1$ μm and $h_s = 525$ μm) at different aspect ratios during heating from room temperature to 200°C: (a) $h/w = 1$, (b) $h/w = 2$, and (c) $h/w = 4$.

theory, as shown in Fig. 8b. Localized stresses in the oxide trench near an interface between the overlying layer are smaller than the stresses in the middle because the trench and the overlying layer are composed of the same material, resulting in essentially no thermal mismatch between them. The localized stresses in the Cu and the oxide lines near the interfaces are expected to nearly cancel each other out. Therefore, curvature changes across the lines from the homogenized composite layer, $\Delta\kappa_y$, which are related to the volume-averaged stresses of the overall layer, $\langle\sigma_{yy}\rangle$, with contributions from both Cu and oxide lines, show good agreement with the theory even down to around $h/w = 1$ (Fig. 6).[22] When the aspect ratio is much higher ($h/w = 4$), the area of the regions where localized stresses are found is smaller, which may explain why FEM results approach the theoretical prediction with increasing aspect ratio.

Effect of Passivation Materials

Table II compares each volume-averaged normal stress component in the Cu lines passivated with either a SiO_2 or a Si_3N_4 layer. In addition to an increase in $\langle\sigma^l_{yy}\rangle$, there is a large increase in $\langle\sigma^l_{zz}\rangle$ when passivated with a Si_3N_4 top layer. In the high-aspect-ratio limit, isostress condition in the y-direction and isostrain condition in the z-direction are assumed. When passivated with a capping layer, isostress condition across the lines is not strictly valid because of localized stress near the interface between the lines and the passivation layer. Passivation, however, causes a favorable effect on the isostrain condition in the out-of-plane direction. These effects in both the y- and z-directions become more pronounced when a stiffer capping layer is deposited.

Figure 10a shows a contour of σ_{zz} in a Cu line and an oxide trench ($h/w = 2$ and $f_l = 0.5$) when passivated with a SiO_2 layer ($h_p/h = 1$). Near the interfaces between under/overlying layers, an isostrain condition in the z-direction does not work well since Cu is likely to have a higher strain than the oxide due to its much higher thermal expansion coefficient relative to SiO_2, even when the lines are passivated with capping materials. The current theory assumes that the strains in the z-direction should be the same, which results in very stiff confinement of the Cu lines in the direction normal to the substrate because Cu tends to expand more than oxide. This leads to an overestimation of the volume-averaged stresses of the Cu lines in the z-direction, $\langle\sigma^l_{zz}\rangle$, compared to the FEM results, as shown in Fig. 8c. Figure 10b shows a contour of σ_{zz} when passivated with Si_3N_4. Because of its higher stiffness, it confines the Cu lines in the z-direction more than the SiO_2 passivation layer. Therefore, it leads to an increase in $\langle\sigma^l_{zz}\rangle$, and the FEM value becomes much closer to the theoretical prediction.

Table II. Comparison of Theoretical Predictions of Volume-Averaged Stresses to Finite Element Results in Cu Lines on Single-Level Structures Without Passivation and with SiO_2 or Si_3N_4 Passivation ($w/p = f_l = 0.5$, $h/w = 2$, $h_p/h = 1$, $h = 1$ μm and $h_s = 525$ μm) During Cooling from 200°C to Room Temperature (Differences from Theory Shown in Parentheses)

	$\langle\sigma^l_{xx}\rangle$ (MPa)	$\langle\sigma^l_{yy}\rangle$ (MPa)	$\langle\sigma^l_{zz}\rangle$ (MPa)	$\langle\sigma^l_h\rangle$ (MPa)
Theory	377	146	180	234
FEM (unpass.)	387 (3%)	161 (10%)	130 (–27%)	226 (–3%)
FEM (SiO_2)	383 (2%)	171 (17%)	157 (–13%)	237 (1%)
FEM (Si_3N_4)	389 (3%)	179 (23%)	169 (–6%)	245 (5%)

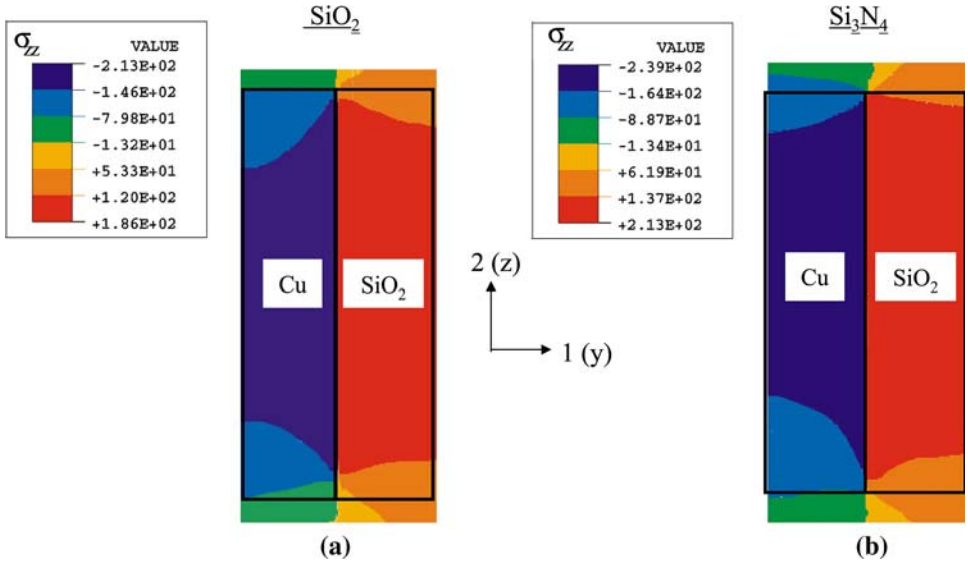

Fig. 10. 2-D FEM contours of stress normal to the substrate, σ_{zz}, on single-level structures with different passivation layers ($w/p = f_l = 0.5$, $h/w = 2$, $h_p/h = 1$, $h = 1$ μm and $h_s = 525$ μm) during heating from room temperature to 200°C: (a) SiO_2 passivation and (b) Si_3N_4 passivation.

Effect of Thermoelastic Properties of Low-k Dielectrics

Based on the analytical solution in this work, volume-averaged thermal stresses in copper interconnect lines and dielectric lines can be computed for lines that are sufficiently tall. Since most low-k dielectrics replacing oxides are polymer-based materials, the relevant elastic constants are typically low. Hydrostatic stresses in lines in a wide range of thermoelastic properties of low-k dielectrics during cooling from 200°C to room temperature are shown in Fig. 11. Assuming that the Poisson's ratios of the dielectrics and the oxide are the same, while they are insensitive to the coefficients of thermal expansion (CTE) of the dielectrics, the thermal stresses in the Cu lines shown in Fig. 11a scale with stiffness of dielectrics, which is in agreement with previous finite element results.[27] Stresses in the dielectrics (Fig. 11b), however, depend on the CTEs as well as the elastic moduli of the dielectric materials. Corresponding stresses from some candidates for low-k dielectrics[28] are indicated to illustrate how the analytical expressions and such maps can be used for selection of dielectric materials in integration with Cu interconnects. Either of a high-modulus/low-CTE material such as tetraethylorthosilane (TEOS) or a low-modulus/high-CTE material such as hydrogen silsesquioxane (HSQ) is compatible with the Cu lines, as far as the thermal stresses in the dielectric lines are concerned.*

*Compatibility issues of low-k dielectrics with Cu metalization associated with stress concentration in via structures will be addressed in another paper.[29]

Effect of Metal Density

Figure 12 shows thermal stresses in Cu lines at a fixed (and high) line aspect ratio ($h/w = 4$) with SiO_2 passivation ($h_p/h = 1$). Lines with high aspect ratio are chosen because they represent the current industrial trend for line geometry in the modern IC industry. Fortuitously, in the high-aspect-ratio case, we can also minimize the effects of localized stresses from under/overlying layers. The validity of the theory at high aspect ratios (tall lines) can then be evaluated explicitly over a wide range of metal density. $\langle\sigma^1_{xx}\rangle$ remains nearly constant with metal density. As metal density increases, however, $\langle\sigma^1_{yy}\rangle$ increases and $\langle\sigma^1_{zz}\rangle$ decreases. As the line structure approaches a continuous Cu film ($w/p = 1$), an equibiaxial stress condition ($\langle\sigma^1_{xx}\rangle = \langle\sigma^1_{yy}\rangle$) with plane stress ($\langle\sigma^1_{zz}\rangle = 0$) is obtained. For tall lines, the current model is in very good agreement with FEM results, especially when the spacing between lines is small. It does, however, show deviation from FEM values as the spacing becomes larger, since oxide lines no longer have high aspect ratios. The ability to predict the effect of metal density at a fixed aspect ratio is one of the advantages of the current model over the Eshelby-type inclusion theory, which is unable to take into account the presence of neighboring lines.[15,16] The stress model for passivated metal lines proposed by Wikström et al.,[17] however, produces very similar values as the model in the current work, over a wide range of metal density. Although their model cannot predict curvature evolution, the assumption that in-plane deformation in lines are totally controlled by substrate deformation seems good as far as volume-averaged stresses are concerned.

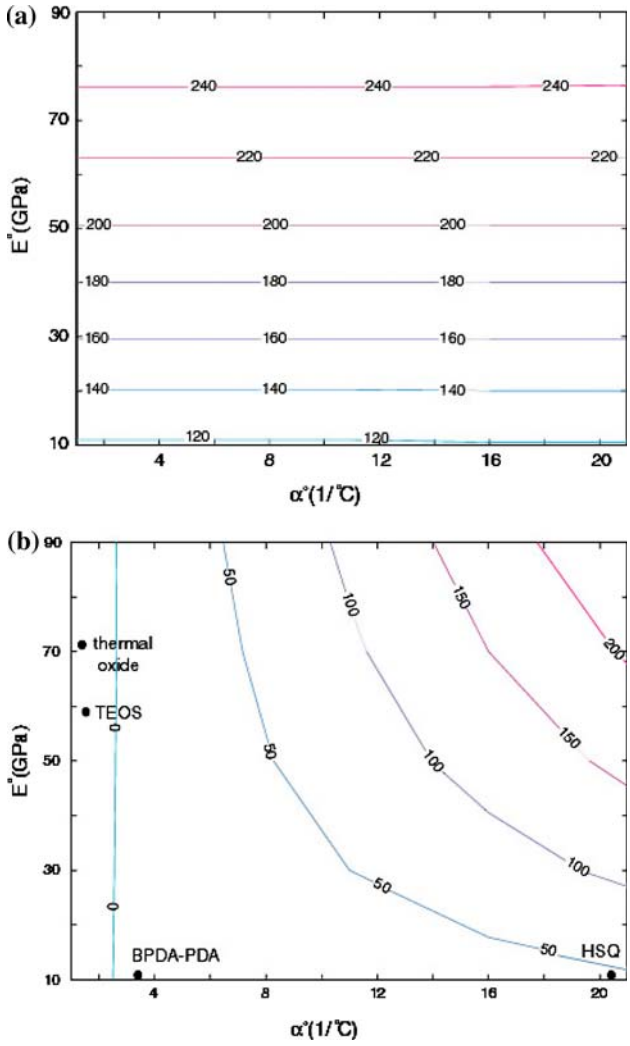

Fig. 11. Analytical predictions of volume-averaged hydrostatic stresses as a function of thermoelastic properties of dielectric materials during cooling from 200°C to room temperature at $f_l = 0.5$: (a) in Cu lines and (b) in dielectric lines.

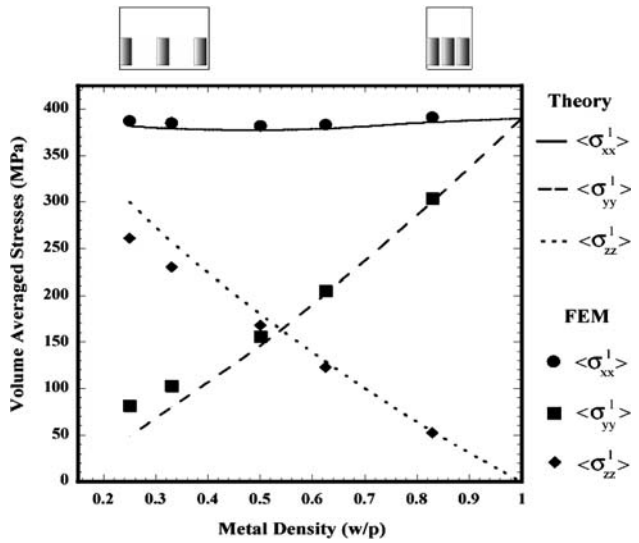

Fig. 12. Volume-averaged stresses in Cu lines on single-level structures with a SiO_2 passivation layer ($h/w = 4$, $h_p/h = 1$, $h = 1$ μm and $h_s = 525$ μm) as a function of metal density (w/p) during cooling from 200°C to room temperature.

Table III. Comparison of Theoretical Predictions of Volume-Averaged Stresses in Cu Lines (with 0.1 μm Si_3N_4 and 0.8 μm SiO_2) to Results of Finite Element Analysis and X-ray Diffraction Experiments ($w/p = f_l = 0.5$, $h/w = 0.7$, $h_p/h = 1.3$, $h = 0.7$ μm and $h_s = 525$ μm) During Cooling from 390°C to Room Temperature

	$\langle\sigma^l_{xx}\rangle$ (MPa)	$\langle\sigma^l_{yy}\rangle$ (MPa)	$\langle\sigma^l_{zz}\rangle$ (MPa)	$\langle\sigma^l_h\rangle$ (MPa)
Theory	806	297	380	494
FEM	727	431	273	477
Experiment	539	459	222	407

Comparison with Experiments

Table III compares theoretical predictions of normal stress components in Cu lines with numerical simulation results in the current work and X-ray diffraction data in a previous report.[8] Since the line aspect ratio of this sample is not exceedingly high ($h/w = 0.7$), it is difficult to compare directly with the theoretical prediction in the high-aspect-ratio limit. The theory's underestimation of $\langle\sigma^l_{yy}\rangle$ and overestimation of $\langle\sigma^l_{zz}\rangle$ compared to FEM values have been discussed previously in the sections "Effect of Line and Passivation Geometry on Stress Evolution" and "Effect of Passivation Materials." Hydrostatic stress, however, which is usually taken to be a key parameter for electromigration simulation,[5] is quite well predicted. Finite element results capture the trend of stress values from X-ray measurement in spite of the complicated line geometry, especially mixed passivation layers of SiO_2 and Si_3N_4. The differences between FEM and experimental results are due to inelastic deformation, such as plastic yielding and/or creep in the lines and anisotropic material properties of Cu, which are not considered in this analysis. It can also be attributed to the low spatial resolution of conventional X-rays (i.e., a spot size that is usually order of magnitude larger than the width of the lines).

Multilevel Structures

In order to capture three-dimensional (3-D) features of the multilevel structure, especially the perpendicular arrangement, a fully 3-D finite element analysis was performed. Results were analyzed to determine whether the curvature predictions are valid for the multilevel structure and to find how thermal stresses vary from level to level. The effects of upper-level line arrangement on stress distribution in lower-level lines are addressed. It is also discussed whether the analytical prediction of thermal stresses based on the

theory in the limiting line geometry of the single layer can be generalized to provide accurate stress estimation in multilevel structures.

Calculation of Curvatures Using Superimposition

Table IV compares theoretical curvature predictions with 3-D FEM results in two different line arrangements following the dual Damascene process shown in Fig. 3. In this calculation, both lower and upper levels have the same line structure ($h/w = 1$ and $f_l = 0.5$). In the aligned structure (Table IVa) the superimposition of three layers, i.e., two composite layers with lines running in the same direction and one ILD layer between them, displays very good agreement of the theory (Eqs. 7 and 8) with the FEM values. In the perpendicular structure (Table IVb) the same curvature values are expected in the x- and y-directions according to the theory due to the symmetry of the structures. This is an expectation which is confirmed by the numerical simulation.

Because of the high diffusivity of Cu through SiO_2 and Si, a diffusion barrier such as TaN is commonly employed between the metal and the dielectric lines.[19] Although this complicates the interconnect structures, the effect of this additional layer can easily be incorporated in the present model by linear superimposition and may be negligible if this layer is very thin, i.e., on the order of a few hundred Ångstroms (e.g., less than 10% of the line width).

Effect of Line Arrangement on Stress Evolution on Lower/Upper Levels

Figure 13 shows contours of hydrostatic stresses during cooling from 200°C to room temperature (20°C) in a two-level Cu interconnect structure without a passivation layer on top of the upper level. This corresponds to the structure after polishing the excess Cu layer on the upper level in the dual Damascene process. In this calculation, both lower and upper levels have the same line structure ($h/w = 1$ and $f_l = 0.5$). For the purpose of comparison, a hydrostatic stress contour of a single-level structure with a passivation layer is shown in Fig. 13a. In the aligned structure (Fig. 13b) the stress values in the Cu line on the upper level are much lower than

Table IV. Comparison of Theoretical Predictions of Curvature Changes of Trilayer Structures (Fig. 3) after the Dual Damascene Process to Finite Element Results ($w/p = f_l = 0.5$, $h/w = 1$, $h_p = 1$ μm, $h = 1$ μm, and $h_s = 525$ μm) During Cooling from 200°C to Room Temperature: (a) Aligned Structure and (b) Perpendicular Structure

	κ_x (l/m)	κ_y (l/m)		κ_x (l/m)	κ_y (l/m)
Theory	0.0394	0.0293	Theory	0.0343	0.0343
FEM	0.0408 (+3.6%)	0.0297 (+1.2%)	FEM	0.0355 (+3.5%)	0.0352 (+26%)

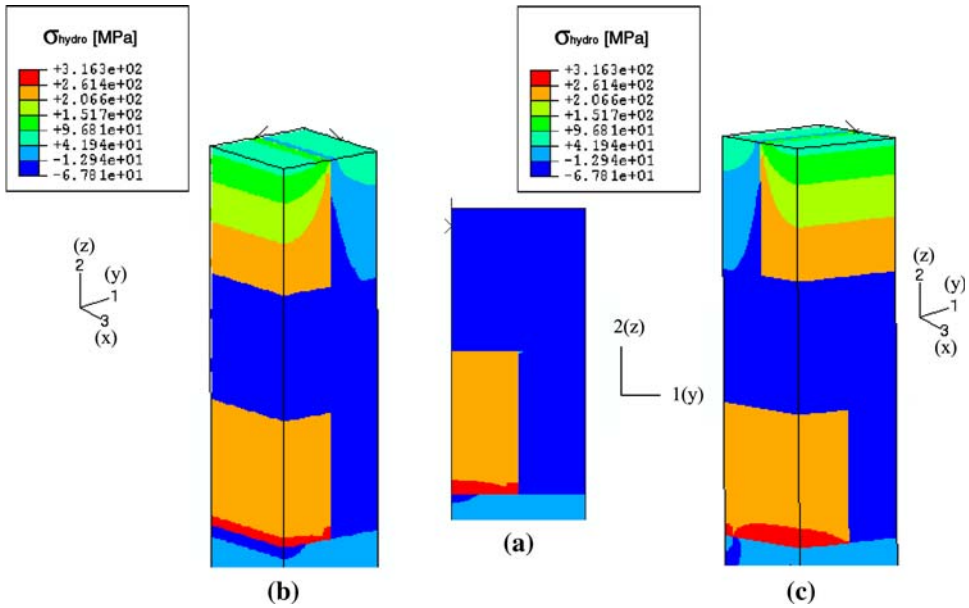

Fig. 13. Contours of hydrostatic stress, σ_{hydro}, during cooling from 200°C to room temperature ($w/p = f_l = 0.5$, $h/w = 1$, $h_p/h = 1$, $h = 1$ μm and $h_s = 525$ μm): (a) single-level with SiO_2 passivation using 2-D FEM, (b) two-level aligned structure, and (c) two-level perpendicular structure after dual Damascene process using 3-D FEM.

those on the lower level. There are two main reasons for the above phenomenon. First, the lines on the upper level are farther from a stiff Si substrate, which relieves stresses, especially in the direction normal to the substrate. In addition, there is no passivation layer on the upper level of the structure after polishing. Therefore, based on the earlier argument, an absence of the passivation layer would reduce stress values in the Cu lines on the upper level. In the perpendicular structure (Fig. 13c) hydrostatic stresses in the lines on the upper level have almost the same values as those in the aligned structure. Furthermore, hydrostatic stresses in the lines on the lower level are not heavily influenced by the presence of the upper level and its arrangement.

Figure 14 shows the contours of von Mises stresses during cooling. Unlike hydrostatic stresses, von Mises stresses are higher in the line on the upper level, except at sharp corners. This is due to the absence of the passivation layer on the upper level because unpassivated Cu lines which are in the dielectric trench with a free top surface may have high deviatoric components unless the aspect ratio is very high. It can also be seen that the upper-level lines show the same results in both the aligned and perpendicular arrangements, and the lower-level lines are hardly affected by the presence and/or arrangement of the upper level. It should be noted, however, that the difference of von Mises stress distribution in the ILD layer can be found in different line arrangements. Typically, the stress values are not exceedingly high, but in general, new insulating materials with low dielectric constants have very low yield strength,[7] which can influence other failure mechanisms, such as yielding in the dielectric.

For the structures in Figs. 13 and 14, volume-averaged values of each normal stress component, hydrostatic, and Mises stresses are summarized in Table V. Compared to a single-level structure, the stress components in the lower-level lines of two-level structures basically remain unchanged, and are independent of the arrangement of the upper-level lines. In the upper lines, however, $\langle \sigma^{l}_{yy} \rangle$ and $\langle \sigma^{l}_{zz} \rangle$ are smaller than those in the lower-level lines. To separate the effects of the relative positions of the lines (whether lines lie on the lower or upper level) from effects of line geometry (whether lines are passivated or not), SiO_2 of the same thickness as the ILD layer was used for the passivation layer on the upper level (Table VI). The upper-level stress values are nearly identical along and across the lines (in-plane stress components) as the lower one, but give slightly smaller values in the stress normal to the substrate (out-of-plane stress component). This is in agreement with a previous result from Shen.[18] This can result from the fact that the upper-level lines are closer to the free surface, so the constraint imposed by the surrounding oxide is not as strong as that experienced by the lower-level lines. There is little difference between the aligned and perpendicular line arrangements. Therefore, it can be seen that interaction between levels in the vertical direction is quite weak when the thickness of the interlevel dielectric (ILD) becomes comparable to that of a metal layer, which is commonly found in practical multilevel structures in the semiconductor industry.

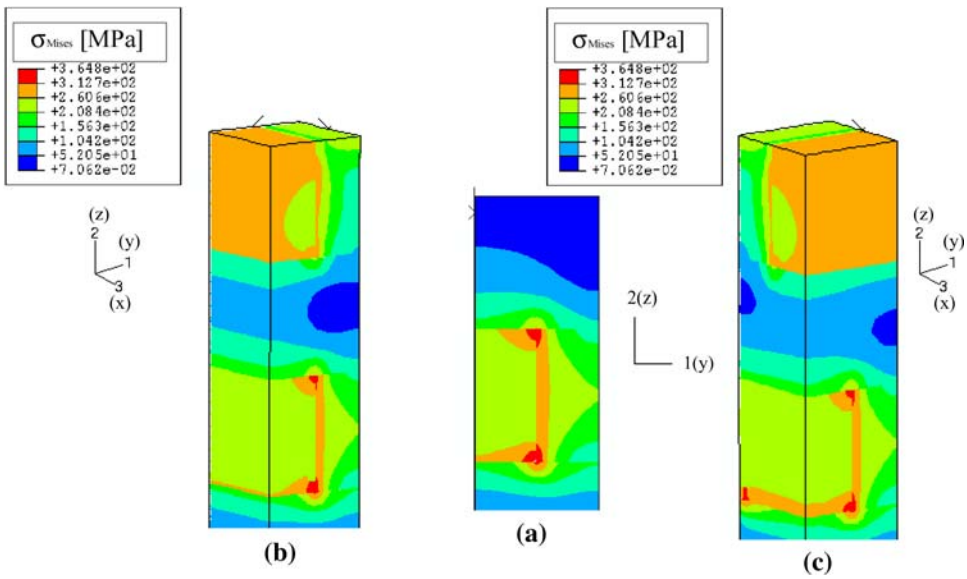

Fig. 14. Contours of von Mises stress, σ_{Mises}, during cooling from 200°C to room temperature ($w/p = f_l = 0.5$, $h/w = 1$, $h_p/h = 1$, $h = 1$ μm and $h_s = 525$ μm): (a) single-level with SiO_2 passivation using 2-D FEM, (b) two-level aligned structure, and (c) two-level perpendicular structure after the dual Damascene process using 3-D FEM.

Table V. Comparison of Volume-Averaged Stresses in Cu Lines on the Single-Metal-Level Structure with SiO_2 Passivation and Two-Metal-Level Structures without Passivation ($w/p = f_l = 0.5$, $h/w = 1$, $h_p = 1$ μm, $h = 1$ μm and $h_s = 525$ μm) During Cooling from 200°C to Room Temperature

		$\langle\sigma^l_{xx}\rangle$ (MPa)	$\langle\sigma^l_{yy}\rangle$ (MPa)	$\langle\sigma^l_{zz}\rangle$ (MPa)	$\langle\sigma^l_h\rangle$ (MPa)	$\langle\sigma^l_{Mises}\rangle$ (MPa)
FEM (single)		387	202	138	242	239
FEM (double; align)	Lower	386	200	139	242	237
	Upper	375	170	81	209	280
FEM (double; perp.)	Lower	386	199	138	241	236
	Upper	373	171	80	208	281

Table VI. Comparison of Volume-Averaged Stresses in Cu Lines on Single-Metal-Level Structure with SiO_2 Passivation and Two-Metal-Level Structures with SiO_2 Passivation ($w/p = f_l = 0.5$, $h/w = 1$, $h_p = 1$ μm, $h = 1$ μm, and $h_s = 525$ μm) During Cooling from 200°C to Room Temperature

		$\langle\sigma^l_{xx}\rangle$ (MPa)	$\langle\sigma^l_{yy}\rangle$ (MPa)	$\langle\sigma^l_{zz}\rangle$ (MPa)	$\langle\sigma^l_h\rangle$ (MPa)	$\langle\sigma^l_{Mises}\rangle$ (MPa)
FEM (single)		387	202	138	242	239
FEM (double; align)	Lower	386	199	139	242	237
	Upper	383	198	131	237	236
FEM (double; perp.)	Lower	385	200	141	241	236
	Upper	375	197	130	234	238

Extension to Four-Level Structure

The finite element analysis of volume-averaged stresses can be extended to a four-level structure with the same line geometry ($h/w = 1$, $h_p/h = 1$ and $f_l = 0.5$) as seen in Table VII. It is clear that the differences from level two to level four in the stress components are negligible. Since Si is much stiffer than SiO_2, the deformation of Cu on the first level is more constrained than those on the other levels. As long as line aspect ratios are sufficiently low or high, this implies that the current theoretical predictions of stress evolution based on the limiting line geometry in the single-level structure are applicable to any level of a multilevel structure, with a slight difference in the out-of-plane stress in the first level on the substrate.

CONCLUSIONS

On the basis of theoretical and numerical analyses carried out in the present work for the single- and multilevel interconnect line structure, the following conclusions are made:

- The interconnect structure comprised of metal and dielectric lines can be characterized by two limiting cases. In the limit of very low aspect ratios, each metal and dielectric line behaves like an individual thin film, and equibiaxial plane stress conditions prevail in each line. When lines are sufficiently tall (high aspect ratio), the line structure is homogenized into a single composite layer with different effective thermoelastic properties along and across the lines due to geometrical anisotropy. The 2-D finite element method using a generalized plane-strain model is in good agreement with the theoretical predictions as the line geometry approaches these limiting cases and also shows a gradual transition at intermediate line aspect ratios.
- When passivated with a capping layer, an isostress condition across the lines is not strictly valid because of localized stresses (mainly interfacial shear stresses) near the interface between the lines and the passivation layer. Passivation, however, has a favorable effect on the isostrain condition in the out-of-plane direction. These effects of passivation become more pronounced as the stiffness of the capping layer increases. In sufficiently tall lines, however, passivation does not make a difference to the stress states in the lines, and the analysis is extremely accurate.
- The current analytical stress model can predict the effect of metal density. It can be shown that the interaction between lines on the same level, i.e., in the lateral direction, is so strong that it cannot be neglected.

Table VII. Comparison of Volume-Averaged Stresses in Cu Lines on Each Level from a Four-Level Structure ($w/p = f_l = 0.5$, $h/w = 1$, $h_p = 1$ μm, $h = 1$ μm, and $h_s = 525$ μm) During Cooling from 200°C to Room Temperature

	$\langle\sigma^l_{xx}\rangle$ (MPa)	$\langle\sigma^l_{yy}\rangle$ (MPa)	$\langle\sigma^l_{zz}\rangle$ (MPa)	$\langle\sigma^l_h\rangle$ (MPa)
FEM (M1)	384	199	139	241
FEM (M2)	381	196	132	236
FEM (M3)	381	196	132	236
FEM (M4)	381	196	131	235

- Comparison of the current model to available experimental data shows reasonable agreement, considering the complicated line geometry, inelastic deformation/anisotropic material properties in the sample, etc.
- From 3-D FEM results of the two-level structure, there is little difference between the aligned and the perpendicular line arrangements. Therefore, it can be seen that the interaction between levels in the vertical direction is quite weak when the thickness of the interlevel dielectric (ILD) layer becomes comparable to that of the metal layer.
- In a multilevel structure, the differences between the stress components in the lines of the second level to those of any other layer (all the way to the top) are negligible. This implies that stress built up in each level is not heavily influenced by the presence of additional layers. This was found to be true when both limiting cases (either flat or tall lines) were approached.

ACKNOWLEDGEMENTS

We acknowledge support of the Defense University Research Initiative on Nano Technology (DURINT) on "Damage- and Failure-Resistant Nanostructured and Interfacial Materials" which is funded of MIT by the Office of Naval Research under Grant N00014-01-1-0808.

REFERENCES

1. M.A. Korhonen, P. Børgesen, K.N. Tu, and C.-Y. Li, *J. Appl. Phys.* 73, 3790 (1993).
2. J.J. Clement and C.V. Thompson, *J. Appl. Phys.* 78, 900 (1995).
3. R.J. Gleixner, B.M. Clemens, and W.D. Nix, *J. Mater. Res.* 12, 2081 (1997).
4. B. Greenbaum, A.I. Sauter, P.A. Flinn, and W.D. Nix, *Appl. Phys. Lett.* 58, 1845 (1991).
5. P. Børgesen, J.K. Lee, R.J. Gleixner, and C.-Y. Li, *Appl. Phys. Lett.* 60, 1706 (1992).
6. D. Kim, W.D. Nix, M.D. Deal, and J.D. Plummer, *J. Mater. Res.* 15, 1709 (2000).
7. S. Chiras and D.R. Clarke, *J. Appl. Phys.* 88, 6302 (2000).
8. T. Marieb, A.S. Mack, N. Cox, D. Gardner, and X.C. Mu, *Mater. Res. Symp. Proc.* 403, 639 (1996).
9. M.A. Moske, P.S. Ho, D.J. Mikalsen, J.J. Cuomo, and R. Rosenberg, *J. Appl. Phys.* 74, 1716 (1993).
10. I.-S. Yeo, S.G.H. Anderson, P.S. Ho, and C.K. Hu, *J. Appl. Phys.* 78, 953 (1995).
11. M.J. Kobrinsky, C.V. Thompson, and M.E. Gross, *J. Appl. Phys.* 89, 91 (2001).
12. Y.-L. Shen, S. Suresh, and I.A. Blech, *J. Appl. Phys.* 80, 1388 (1996).
13. A. Gouldstone, Y.-L. Shen, S. Suresh, and C.V. Thompson, *J. Mater. Res.* 13, 1956 (1998).
14. E.S. Ege and Y.-L. Shen, *J. Electron. Mater.* 32, 1000 (2003).
15. H. Niwa, H. Yagi, H. Tsuchikawa, and M. Kato, *J. Appl. Phys.* 68, 328 (1990).
16. M.A. Korhonen, R.D. Black, and C.-Y. Li, *J. Appl. Phys.* 69, 1748 (1991).
17. A. Wikström, P. Gudmundson, and S. Suresh, *J. Appl. Phys.* 86, 6088 (1999).
18. Y.-L. Shen, *J. Mater. Res.* 12, 2219 (1997).
19. N. Misawa, T. Ohba, and H. Yagi, *MRS Bull.* 19, 63 (1994).
20. G.G. Stoney, *Proc. R. Soc. Lond.* A82, 172 (1909).
21. M. Finot and S. Suresh, *J. Mech. Phys. Solids* 44, 683 (1996).
22. T.-S. Park and S. Suresh, *Acta Mater.* 48, 3169 (2000).
23. A. Wikström, P. Gudmundson, and S. Suresh, *J. Mech. Phys. Solids* 47, 1113 (1999).
24. A. Wikström and P. Gudmundson, *Acta Mater.* 48, 2429 (2000).
25. L.B. Freund and S. Suresh, *Thin Film Materials; Stress, Defect Formation, and Surface Evolution*, Chap. 3 (UK: Cambridge University Press, 2004).
26. ABAQUS Version 6.1, general purpose finite element program, Hibbit, Karlson and Sorensen Inc., Pawtucket, RI, USA (2000).
27. S.P. Hau-Riege and C.V. Thompson, *J. Mater. Res.* 15, 1797 (2000).
28. J.-H. Zhao, T. Ryan, P.S. Ho, A.J. McKerrow, and W.-Y. Shih, *J. Appl. Phys.* 88, 3029 (2000).
29. A.J. Rosakis, T.-S. Park, and S. Suresh, *Thin Solid Films* (Submitted).